An Analysis of Conditions Associated with an Occurrence of Stratospheric CAT[1]

RICHARD D. DELAY

Captain, Air Weather Service, U. S. Air Force

AND JOHN A. DUTTON

Dept. of Meteorology, The Pennsylvania State University, University Park

(Manuscript received 29 April 1971)

ABSTRACT

Cross sections of potential temperature, wind shear, and gradient Richardson number were constructed from data obtained during a Project HICAT flight and analyzed to determine the relationship to clear air turbulence in the stratosphere. CAT was found to be associated with strong baroclinic zones and with a critical value of the Richardson number of 0.25.

Energy budgets for five patches of turbulence associated with this outbreak of stratospheric clear air turbulence were also examined, and found to balance within 4–18% of the total rate of shear production.

1. Introduction

It is now well known that clear air turbulence (CAT) poses a serious threat to aircraft flights in the lower stratosphere, and that mathematical models of the atmosphere must include the effects of CAT. However, before clear air turbulence can be predicted accurately, or its effects incorporated in a numerical model, the physical processes and the atmospheric conditions associated with CAT must be better understood.

Studies have shown that CAT is found in the upper troposphere and lower stratosphere, with more occurrences over the mountains, in regions of large stability and strong wind shear. Reiter (1969) pointed out that CAT is sporadic and patchy in nature, with most patches having horizontal dimensions <37 km. He concluded that the mesoscale structure of the atmosphere is important in the generation of clear air turbulence. Atlas *et al.* (1970) used ultra-high-resolution radars to observe low-altitude, amplifying and breaking waves, similar to those resulting from Kelvin-Helmholtz instability. Quantitative measurements of signal strength indicated that the turbulent eddies occurred in short thin layers.

A commonly used indicator of probable turbulent areas is the gradient Richardson number, Ri. Dutton and Panofsky (1970) pointed out that the probability of finding clear air turbulence is increased in those regions where the gradient Richardson number is small. Theoretical studies of instability in incompressible fluids indicate that the critical value of the Richardson number is 0.25, and Dutton and Fichtl (1969) extended these theoretical results to the atmospheric case.

Attempts at analyzing synoptic-scale data to determine the average atmospheric conditions associated with turbulence and a critical value of the Richardson number are hampered by three problems: 1) the soundings are too far apart to resolve the mesoscale phenomenon associated with CAT, 2) time differences of up to 6 hr may exist between radiosonde soundings and the occurrence of turbulence, and 3) the turbulence may occur hundreds of miles away from any sounding. Axford (1968) demonstrated that aircraft can be used to obtain mesoscale variations of vertical wind shear and thus serve as the prime data source for the smaller scale ambient features found in and around turbulent areas.

This study suggests that aircraft measurements may be used as the prime source of data for analysis of both clear air turbulence and the associated ambient conditions. The relationships between CAT, baroclinic zones, and Richardson number are examined using cross sections constructed from aircraft data. We present a vertical cross section of gradient Richardson number in the stratosphere, and examine the energy budgets for five turbulent layers.

2. Method of analysis

The data used to construct the cross sections in this study are 1-min averages computed from continuous time histories of corrected pressure altitude, ambient air temperature, wind direction, wind magnitude, and horizontal position coordinates. Two factors made possible the construction of a cross section from single

[1] The views expressed herein are those of the authors and do not necessarily reflect those of Air University, the United States Air Force or the Department of Defense.

aircraft data. First, the pilot did not maintain an exact altitude; instead, the altitude of the aircraft varied between 60,200 and 61,800 ft. Second, the static stability of the stratosphere guarantees that potential temperature increases with height. Fig. 1 is an example of how these two factors can be combined to construct an isentropic cross section. The potential temperature was calculated and plotted as a function of the position of the aircraft, indicated by solid circles. Isentropes were then drawn using the fact that potential temperature increases with height in the stratosphere and continuity was then used to draw some isentropes above and below the flight path. As in all meteorological analyses, some subjectivity was necessarily involved.

There are obvious limitations of the cross sections. The first is the restriction to two dimensions because there is no way to determine the extent of the turbulence in any direction other than along the flight path of the aircraft. The second is that the accuracy of the analyses decreases as a function of the distance from the actual flight path. As a result, the most representative portions of the cross sections are along and in the immediate vicinity of the flight path where the data points are located.

For use in this study, the gradient Richardson number

$$\mathrm{Ri}=\frac{g}{\theta}\frac{\partial\theta}{\partial z}\left|\frac{\partial \mathbf{V}}{\partial z}\right|^{-2} \tag{1}$$

can be written in the form

$$\mathrm{Ri}=-\frac{R}{p^{c_v/c_p}p_0^{R/c_p}}\frac{\partial\theta}{\partial p}\left|\frac{\partial \mathbf{V}}{\partial p}\right|^{-2}, \tag{2}$$

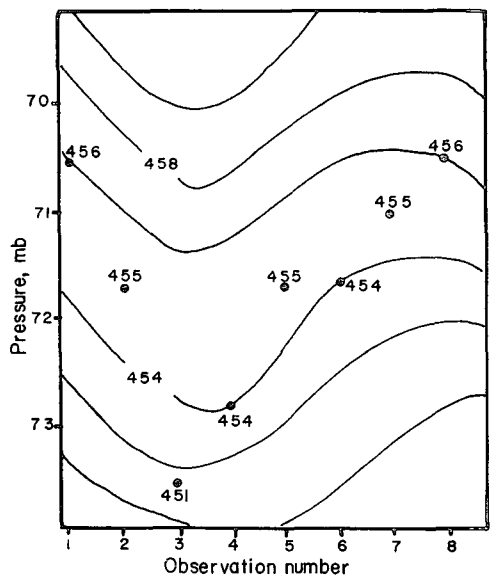

FIG. 1. Example of the method used in the isentropic cross-sectional analysis. See text for discussion.

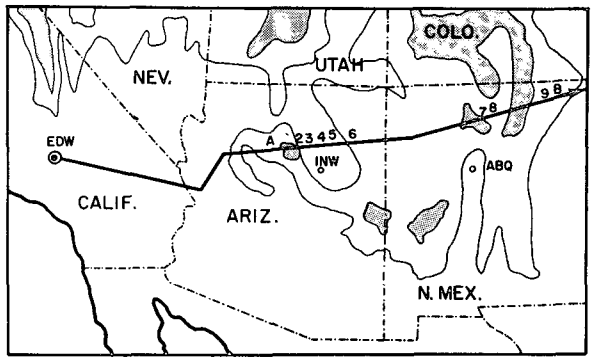

FIG. 2. Flight path and turbulence encounters (2 through 9). Stippled areas indicate an elevation greater than 9000 ft. The clear areas enclosed by the other contours indicate elevations of 6000–9000 ft, while areas outside these contours represent elevations less than 6000 ft.

using the hydrostatic approximation. The wind vector $\mathbf{V}$ can be written as

$$\mathbf{V}=\mathbf{i}V\cos\Phi+\mathbf{j}V\sin\Phi, \tag{3}$$

where Φ is the angle in radians between the vector $\mathbf{V}$ and the unit vector $\mathbf{i}$, and V is the magnitude of $\mathbf{V}$. If (3) is differentiated partially with respect to pressure and squared, then

$$\left|\frac{\partial \mathbf{V}}{\partial p}\right|^2=\left(\frac{\partial \mathbf{V}}{\partial p}\right)^2+V^2\left(\frac{1}{57}\frac{\partial\psi}{\partial p}\right)^2, \tag{4}$$

where Ψ is the angle in degrees. With (4) the equation for the gradient Richardson number can be written in the form

$$\mathrm{Ri}=-\frac{R}{p^{c_v/c_p}p_0^{R/c_p}}\frac{\partial\theta}{\partial p}\Big/\left[\left|\frac{\partial \mathbf{V}}{\partial p}\right|^2+V^2\left(\frac{1}{57}\frac{\partial\Psi}{\partial p}\right)^2\right]. \tag{5}$$

The field of Richardson numbers can then be calculated using (5) and the cross sections of potential temperature, wind speed and wind direction.

3. The case study

The data used in this study were obtained by a Project HICAT ferry flight, number 180, from Edwards AFB, Calif., to Hanscom Field, Mass., on 13 March 1967. The aircraft was equipped with an inertially stabilized turbulence measurement system and inertial equipment for determination of the ambient wind field. Fig. 2 shows the portion of the flight path analyzed, starting at point A and terminating at point B, a distance of 660 km. The location of the turbulence occurrences analyzed here are shown in the figure using numbers from 2 through 9, each number being identified as a turbulence event. Table 1 summarizes the meteorological conditions at the time of turbulence and the severity of turbulence as encountered by the aircraft (Crooks *et al.*, 1968).

TABLE 1. Summary of turbulence encounters and associated meteorological conditions for HICAT flight 180 on 13 March 1967. All encounters were associated with mountainous terrain.

Event number	Time (GMT)	Duration of turbulence (sec)	Average altitude (ft)	Average wind (deg/kt)	Average temperature (°C)	Turbulence intensity*
2	1903	90	61,300	229/43	−59.5	2
3	1905	40	61,000		−59.1	2
4	1906	110	61,300	254/32	−58.5	1–2
5	1909	125	61,300	249/28	−58.8	2–3
6	1916	50	61,000		−57.7	2
7	1935	145	60,900	254/23	−59.8	1–2
8	1939	27	60,200		−59.6	1–2
9	1947	130	60,800	256/44	−58.1	1

* 1–light; 2–moderate; 3–severe.

An analysis of the wind profiles shows that synoptic conditions favored the formation of lee waves in the area under study. As can be seen from Fig. 3 and Table 2, the winds over Albuquerque and Winslow increased in speed with height to a maximum of 91 kt at 200 mb, maintaining a direction such that the flow was normal to the mountains. Thus, conditions were favorable for lee wave activity north of Albuquerque and Winslow.

Figs. 4a and b are the isentropic cross sections obtained by analysis of the aircraft data, each interval on the abscissa representing 1 min (~13 km); the turbulent events listed in Table 1 are identified by Roman numerals. All of the events are related to strong baroclinic zones, with encounter number 5, the longest and most severe, occurring on the upwind side of the largest wave-like perturbation. The perturbations appearing in the analysis are possibly the result of mountain wave activity extending into the stratosphere. This hypothesis is supported by the favorable conditions existing for the development of lee waves and by the location of the waves on the lee side of the mountain ranges. The largest perturbation has a wavelength of ~110 km. Thus, it would appear that any attempts at accurately locating zones of turbulence, using baroclinicity as an indicator, will require measurements of atmospheric variables on a scale smaller than the present synoptic-scale sounding network.

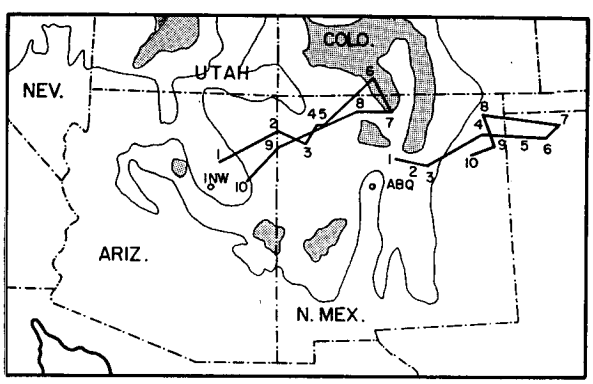

FIG. 3. Hodographs for Winslow and Albuquerque soundings for 1200 GMT 13 March 1967. Elevations are as given in Fig. 2.

Figs. 5a and b show the cross sections of wind direction (Ψ), while Figs. 6a and b give those of wind magnitude (V). The largest change of wind direction occurred in the vicinity of the first three turbulent encounters. With the exception of event number 8, all events occurred in areas of strong vertical wind shear. Common to both cross sections are the small-scale variations in the wind fields which would not appear in synoptic-scale analyses. Phillips (1967) suggests that the turbulence should occur preferentially at either the crest or trough of a wave when strong wind shear is present. Although, this was not observed in this study a strong correlation was found between wind shear and turbulence.

Figs. 7a and b show the cross sections of gradient Richardson numbers. All of the turbulent events occurred when the aircraft traversed regions where the values of Richardson number were less than 0.25. These areas of low Richardson number coincide with the occurrence of mesoscale perturbations in the

TABLE 2. Radiosonde observed winds at mandatory levels.

Observation	Pressure	Altitude (ft)	Wind (deg/kt)
Winslow, Ariz., 1200 GMT 13 March 1967			
1	800	6,396	205/12
2	700	9,938	235/44
3	600	13,972	246/50
4	500	18,564	245/58
5	400	23,976	243/42
6	300	30,569	246/91
7	200	39,163	250/91
8	100	53,201	246/46
9	80	57,662	244/35
10	70	60,384	267/17
Albuquerque, N. M., 1200 GMT 13 March 1967			
1	800	6,494	254/13
2	700	12,300	262/25
3	600	14,104	263/29
4	500	18,663	255/54
5	400	24,075	260/68
6	300	30,733	263/81
7	200	39,360	260/91
8	100	53,431	248/58
9	80	57,859	258/60
10	70	60,516	260/48

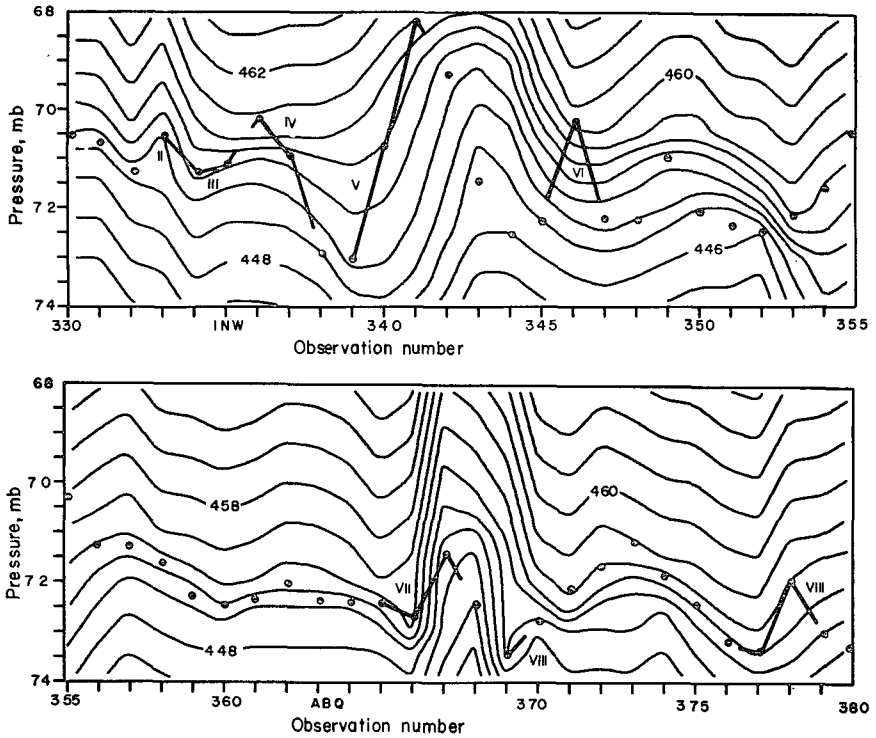

FIG. 4. Isentropic cross-sectional analysis along the flight path of 13 March 1967. Each interval on the abscissa represents 1 min, or since the velocity of the aircraft was approximately constant, a distance of about 13 km. The flight path of the aircraft is depicted by solid circles and the areas in which turbulence occurred by solid lines connecting the circles. As a result of scaling, all slopes are enlarged by a factor of 372. Note that the last roman numeral in the bottom figure should be IX.

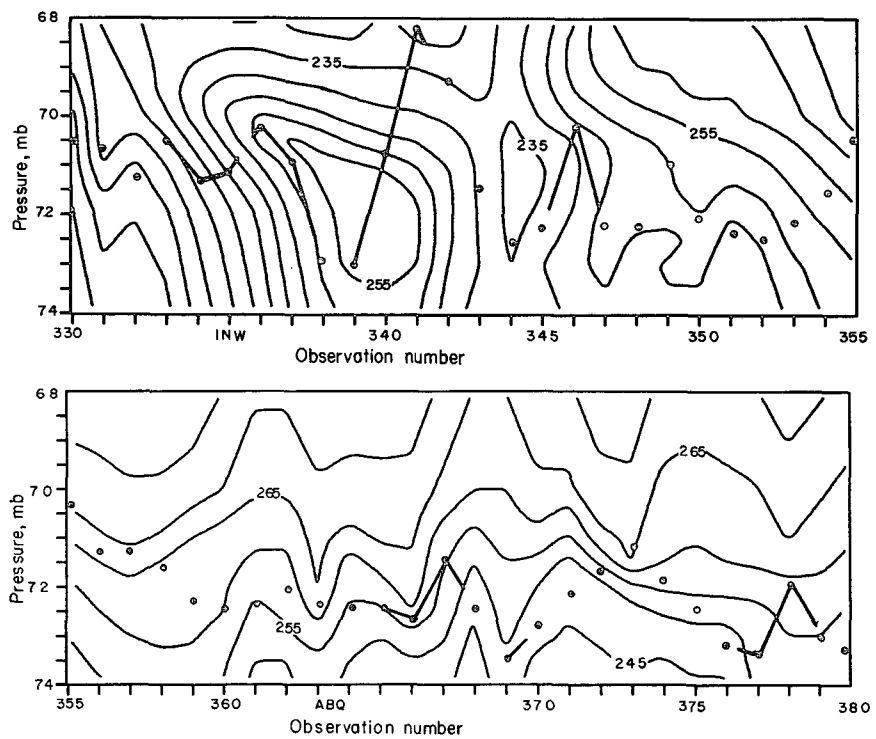

FIG. 5. Cross section of wind direction along the flight path of 13 March 1967. See legend to Fig. 4.

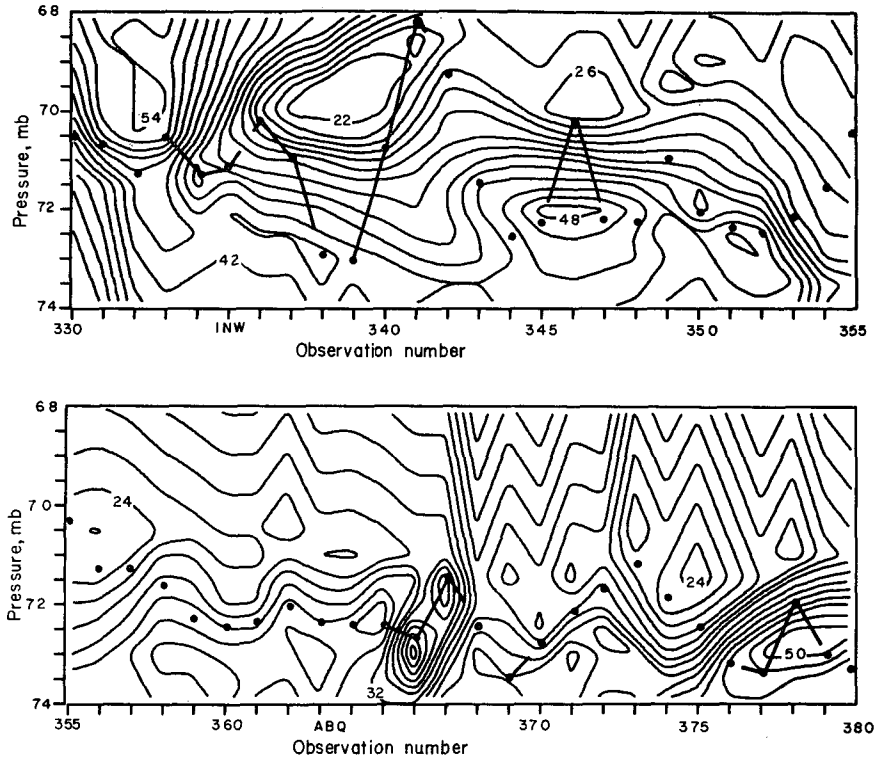

FIG. 6. Cross section of wind speed (kt) along the flight path of 13 March 1967. See legend to Fig. 4.

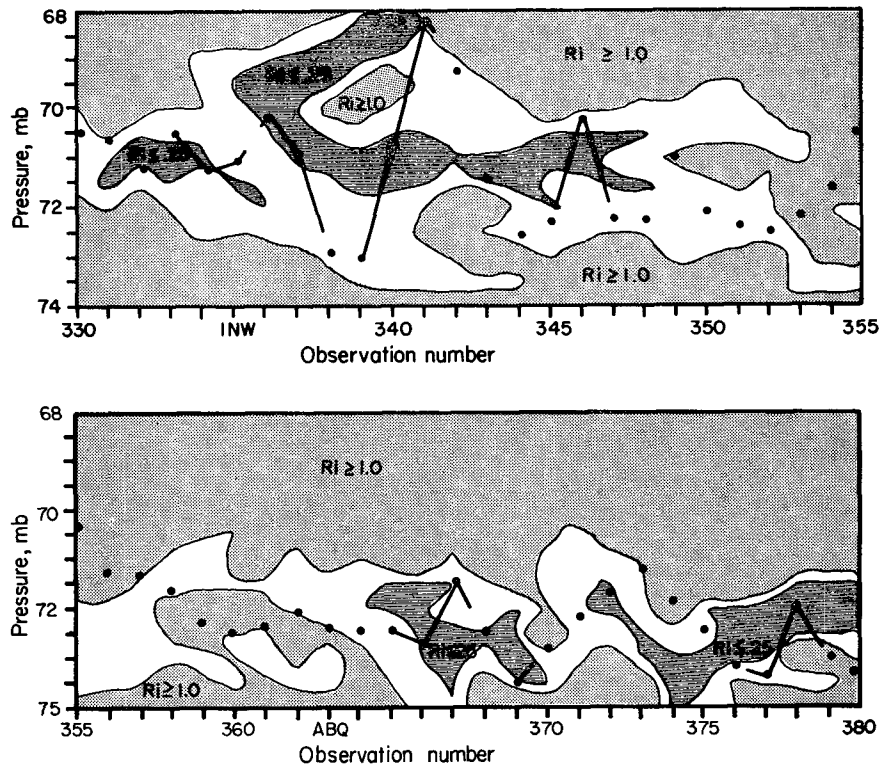

FIG. 7. Cross section of gradient Richardson number along the flight path of 13 March 1967. See legend to Fig. 4.

potential temperature fields. A distinctive feature of the analysis is the thin, patchy distribution of Richardson numbers <0.25. This distribution of low Ri values, and the turbulence associated with it, would be impossible to detect using a synoptic-scale analysis. It is interesting to note that this thin, erratic distribution is in agreement with recent observations of turbulent regions in the lower atmosphere (Atlas *et al.*, 1970).

4. Energy budget analysis

The equation of motion can be written in the form

$$\frac{\partial v_i}{\partial t}+v_k\frac{\partial v_i}{\partial x_k}=f_i, \quad i=1, 2, 3. \tag{6}$$

Modern flight data on wind velocities v_i include a high-frequency component u_i which is a reliable estimate of the turbulent component of the velocity, and a slowly varying component U_i that represents the mesoscale structure of the atmosphere in which the turbulence is embedded. The forces f_i can also be represented by a slowly varying component K_i and a fluctuating component k_i. Thus, we assume that

$$v_i=U_i+u_i, \quad f_i=K_i+k_i. \tag{7}$$

Lester (1970) points out that without a spectral gap between the high- and low-frequency components of velocity, interactions between the components become important in the computation of an energy budget. For the purpose of this study it is assumed either that u_i and U_i are produced from the same system and are isolated by filtering, or that u_i is produced by a turbulence measurement system and U_i by a low-frequency system, such as a Doppler radar designed to measure wind. As a consequence of the filtering and preliminary data conditioning, it is generally true that

$$\overline{u_i}=0, \quad \overline{k_i}=0, \tag{8}$$

where the overbar denotes an average over a particular data sample. However, in contrast to the simpler case of turbulence in a homogeneous average wind field, as often occurs in the atmosphere boundary layer, it cannot be assumed for an arbitrary operation h, that

$$\overline{u_i h(U_j)}=0. \tag{9}$$

However, it is true that

$$\overline{u_i h(\bar{U}_j)}=0. \tag{10}$$

The combinations of Eqs. (6) and (7) thus gives

$$\frac{\partial U_i}{\partial t}+\frac{\partial u_i}{\partial t}+U_k\frac{\partial U_i}{\partial x_k}+U_k\frac{\partial u_i}{\partial x_k}+u_k\frac{\partial U_i}{\partial x_k}+u_k\frac{\partial u_i}{\partial x_k}=K_i+k_i. \tag{11}$$

If the mean of (11) is subtracted from (11), then

$$\frac{\partial}{\partial t}(u_i+U_i')+U_k\frac{\partial U_i}{\partial x_k}-\overline{U_k\frac{\partial U_i}{\partial x_k}}+U_k\frac{\partial u_i}{\partial x_k}-\overline{U_k\frac{\partial u_i}{\partial x_k}}+u_k\frac{\partial U_i}{\partial x_k}-\overline{u_k\frac{\partial U_i}{\partial x_k}}+u_k\frac{\partial u_i}{\partial x_k}-\overline{u_k\frac{\partial u_i}{\partial x_k}}=k_i+K_i', \tag{12}$$

where

$$U_i'=U_i-\overline{U_i}, \quad K_i'=K_i-\overline{K_i}. \tag{13}$$

If (12) is multiplied by u_i and averaged, we have

$$\overline{\frac{\partial u_i^2/2}{\partial t}}+\overline{u_i\frac{\partial U_i'}{\partial t}}+\overline{u_iU_k\frac{\partial U_i}{\partial x_k}}+\overline{U_k\frac{\partial u_i^2/2}{\partial x_k}}+\overline{u_iu_k\frac{\partial U_i}{\partial x_k}}+\overline{u_iu_k\frac{\partial u_i}{\partial x_k}}=\overline{u_i(k_i+K_i')}. \tag{14}$$

The kinetic energy $\bar{e}$ is

$$\bar{e}=\overline{u_i^2/2}=\tfrac{1}{2}\overline{(u^2+v^2+w^2)}, \tag{15}$$

so that (14) becomes

$$\frac{\partial\bar{e}}{\partial t}=-\overline{u_iu_k\frac{\partial U_i}{\partial x_k}}-\overline{u_i\frac{\partial U_i'}{\partial t}}-\overline{u_iU_k\frac{\partial U_i}{\partial x_k}}-\overline{U_k\frac{\partial e}{\partial x_k}}-\overline{u_k\frac{\partial e}{\partial x_k}}+\overline{u_i(k_i+K_i')}. \tag{16}$$

It can be shown (Lumley and Panofsky, 1964; Dutton and Fichtl, 1969) that

$$\overline{u_i(k_i+K_i')}=g\overline{\frac{u_3T'}{T_0}}-\overline{\frac{\partial}{\partial x_k}p'u_k}-\bar{\epsilon}, \tag{17}$$

where $\bar{\epsilon}$ represents dissipation by viscous forces. Thus, (16) can be written as

$$\frac{\partial\bar{e}}{\partial t}=-\overline{u_iu_k\frac{\partial U_i}{\partial x_k}}+g\overline{\frac{u_3T'}{T_0}}-\bar{\epsilon}-\overline{\frac{\partial}{\partial x_k}p'u_k}-\overline{u_i\frac{\partial U_i'}{\partial t}}-\overline{u_iU_k\frac{\partial U_i}{\partial x_k}}-\overline{U_k\frac{\partial e}{\partial x_k}}-\overline{u_k\frac{\partial e}{\partial x_k}}. \tag{18}$$

The first term on the right side of (18) can be expanded to

$$\overline{u_iu_k\frac{\partial U_i}{\partial x_k}}=\overline{u_1u_3\frac{\partial U_1}{\partial x_3}}+\overline{u_2u_3\frac{\partial U_2}{\partial x_3}}+\overline{u_1^2\frac{\partial U_1}{\partial x_1}}+\overline{u_2u_1\frac{\partial U_2}{\partial x_1}}+\overline{u_1u_2\frac{\partial U_1}{\partial x_2}}+\overline{u_2^2\frac{\partial U_2}{\partial x_2}}+\overline{u_3u_1\frac{\partial U_3}{\partial x_1}}+\overline{u_3u_2\frac{\partial U_3}{\partial x_2}}+\overline{u_3^2\frac{\partial U_3}{\partial x_3}}. \tag{19}$$

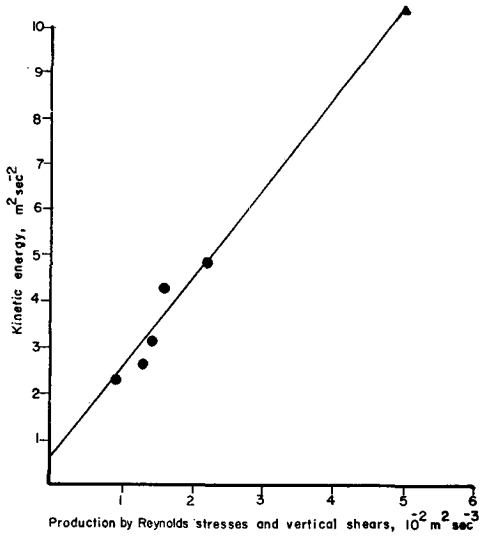

FIG. 8. Kinetic energy vs production by Reynolds stresses and vertical shears. See text for discussion.

With the data used in this study, which was not collected with an energy budget analysis in mind, only the first four terms on the right side of (19) can be calculated. We thus resubstitute (19) into (18) and combine all terms except the four Reynolds stresses, the buoyancy term, and the dissipation into a residual term R. The terms in (18) such as $\overline{u_1 \partial(U_1^2/2)/\partial x_1}$ and the advection of e are also in R. This gives the final equation

$$R = -\overline{u_1 u_3}\frac{\partial U_1}{\partial x_3} - \overline{u_2 u_3}\frac{\partial U_2}{\partial x_3} - \overline{u_1^2}\frac{\partial U_1}{\partial x_1} - \overline{u_2 u_1}\frac{\partial U_2}{\partial x_1} + g\frac{\overline{u_3 T'}}{T_0} - \bar{\epsilon}. \quad (20)$$

The energy budgets for five of the eight stratospheric turbulence events were analyzed using (20). The variances and covariances were calculated from the time histories of gust velocity measurements and fast response temperature measurements, after removal of linear trends. The shears of the slowly varying wind components were calculated from the cross sections, and the dissipation from the energy spectra utilizing inertial subrange theory. Each turbulence event was analyzed at 20-sec intervals. The terms in the energy equation (20) were calculated for each interval and then averaged over the whole event. Table 3 is a summary of the results. As can be seen, turbulent energy production by vertical shear is considerably larger than that due to horizontal shear in all cases. Table 3 also shows that the residual in the energy budget for all five turbulence events was within 4–18% of the total due to shear production.

TABLE 3. Summary of energy budget analyses. Units are 10^{-2} m² sec^{-3} unless otherwise specified.

Event number	2	4	5	7	9
Production by Reynolds stresses and vertical shears	2.23	1.48	0.89	1.51	1.29
Production by Reynolds stresses and horizontal shears	0.72	−0.12	0.04	0.12	0.02
Total Production by Reynolds stresses and shears	2.95	1.36	0.93	1.63	1.31
Buoyancy production	0.06	0.11	0.00	−0.59	−0.72
Dissipation	−2.46	−1.58	−0.85	−0.97	−0.67
Residual	0.55	−0.11	0.08	0.07	−0.08
Flux Richardson number	−0.02	−0.08	0.00	0.36	0.55
Kinetic energy (m² sec^{-2})	4.90	3.21	2.30	4.20	2.60

An interesting result of this analysis is the approximately linear relationship between kinetic energy and turbulent energy production by Reynolds stresses and vertical shears shown in Fig. 8. The five points in the lower left are from the five turbulence events analyzed in this study. The value in the upper right was obtained by Dutton (1969) in a study of an energy budget of a layer of stratospheric clear air turbulence.

5. Summary

Stratospheric clear air turbulence was found to be closely associated with areas of strong baroclinicity and vertical shear. The critical value of Richardson number in the stratosphere appears to be in agreement with the value arrived at in theoretical studies, namely, 0.25. Furthermore, the distribution of Richardson number, baroclinic zones, and wind shear in the stratosphere is patchy, erratic, and mesoscale in nature. Therefore, any attempts at understanding the physical processes of clear air turbulence in the stratosphere will require data collected on a scale much smaller than that of the present synoptic network.

Detailed analysis of the energy budget of clear air turbulence is clearly possible with high quality aircraft data. The production of turbulent energy by Reynolds stresses in layers of CAT appears to be almost balanced by the dissipation due to viscous forces. There also appears to be a linear correlation between kinetic energy and the production of turbulent energy by Reynolds stresses and vertical shear, but no attempt is made at this time to explain this correlation.

Acknowledgments. A number of persons assisted in making data available for this study; these include Walter M. Crooks of Lockheed-California, Burbank, Calif., Frank Lewis of the Techniques Development Laboratory, National Weather Service, Washington, D. C., and J. P. Boone of the Flight Dynamics Laboratory, Wright-Patterson Air Force Base, Ohio. The authors would also like to thank Prof. Hans A. Panofsky of The Pennsylvania State University for his discussion and advice during the course of this study.

The research reported here was supported in part by the National Science Foundation under Grant 1595X to The Pennsylvania State University.

REFERENCES

Atlas, D., J. I. Metcalf, J. H. Richter and E. E. Gossard, 1970: The birth of "CAT" and microscale turbulence. *J. Atmos. Sci.*, **27**, 903–913.

Axford, D. N., 1968: On the accuracy of wind measurements using an inertial platform in an aircraft, and an example of a measurement of the vertical mesostructure of the atmosphere. *J. Appl. Meteor.*, **7**, 645–666.

Crooks, W. M., F. M. Hoblit, F. A. Mitchell, *et al.*, 1968: Project HICAT—High altitude measurements and meteorological correlations. Tech. Rept. AFFDL-TR-68-12, Vol. I, Air Force Flight Dynamics Laboratory, Wright-Patterson Air Force Base, Ohio.

Dutton, J. A., 1969: An energy budget for a layer of stratospheric CAT. *Radio Sci.*, **4**, 1137–1142.

——, and G. H. Fichtl, 1969: Approximate equations of motion for gases and liquids. *J. Atmos. Sci.*, **26**, 241–254.

——, and H. A. Panofsky, 1970: Clear air turbulence: A mystery may be unfolding. *Science*, **167**, 937–944.

Lester, P. F., 1970: Some physical and statistical aspects of clear air turbulence. Atmos. Sci. Paper No. 165, Colorado State University, Fort Collins.

Lumley, J. L., and H. A. Panofsky, 1964: *The Structure of Atmospheric Turbulence.* New York, Interscience Publ., 239 pp.

Phillips, O. M., 1967: The generation of clear air turbulence by the degradation of internal waves. *Atmospheric Turbulence and Radio Wave Propagation*, Nauka, Moscow.

Reiter, E. R., 1969: The nature of clear air turbulence: A review. *Clear Air Turbulence and Its Detection*, New York, Plenum Press, 7–32.